ACS APPLIED MATERIALS & INTERFACES

Article

Using p-Type PbS Quantum Dots to Quench Photocurrent of Fullerene-Au NP@MoS2 Composite Structure for Ultrasensitive Photoelectrochemical Detection of ATP

Mengjie Li, Yingning Zheng, Wenbin Liang, Ruo Yuan, and Ya-Qin Chai

ACS Appl. Mater. Interfaces, **Just Accepted Manuscript** • DOI: 10.1021/acsami.7b13894 • Publication Date (Web): 07 Nov 2017

Just Accepted

ACS Publications

ACS Applied Materials & Interfaces is published by the American Chemical Society.
1155 Sixteenth Street N.W., Washington, DC 20036

Using p-Type PbS Quantum Dots to Quench Photocurrent of Fullerene-Au NP@MoS_2 Composite Structure for Ultrasensitive Photoelectrochemical Detection of ATP

Meng-Jie Li, Ying-Ning Zheng, Wen-Bin Liang, Ruo Yuan, Ya-Qin Chai**

Key Laboratory of Luminescent and Real-Time Analytical Chemistry (Southwest University), Ministry of Education, College of Chemistry and Chemical Engineering, Southwest University, Chongqing 400715, PR China

ABSTRACT: The ultrasensitive and rapid quantification of the universal energy currency adenosine triphosphate (ATP) is an extremely critical mission in field of clinical applications. In this work, a "signal-off" photoelectochemical (PEC) biosensor was designed for ultrasensitive ATP detection based on a fullerene (C_{60}) decorated Au nanoparticle@MoS_2 (C_{60}-Au NP@MoS_2) composite material as a signal indicator and a p-type PbS quantum dot (QD) as an efficient signal quencher. Modification of wide band gap C_{60} with narrow band gap MoS_2 to form an ideal PEC signal indicator was proposed, which could significantly improve photo-current conversion efficiency, leading to a desirable PEC signal. In the presence of p-type PbS QDs, the PEC signal of n-type C_{60}-Au NP@MoS_2 was effectively quenched,

*Corresponding authors at: Tel.: +86-23-68252277, fax: +86-23-68253172.

E-mail addresses: yuanruo@swu.edu.cn (R. Yuan); yqchai@swu.edu.cn (Y. Q. Chai)

because p-type PbS QDs could compete with C_{60}-Au NP@MoS_2 to consume light energy and electron donor. Besides, the conversion of a limited amount of target ATP into an amplified output PbS QD-labeled short DNA sequence (output S_1) was achieved *via* target mediated aptazyme cycling amplification strategy, facilitating ultrasensitive ATP detection. The proposed "signal-off" PEC strategy exhibited a wide linear range from 1.00×10^{-2} pM to 100 nM with a low detection limit of 3.30 fM. Importantly, this proposed strategy provides a promising platform to detect ATP at ultralow levels, and has potential applications including diagnosis of ATP-related diseases, monitoring of diseases progression and evaluation of prognosis.

KEYWORDS: Adenosine triphosphate; Photoelectochemical biosensor; Fullerene decorated Au nanoparticle@MoS_2; Signal indicator; P-type PbS quantum dots; Signal quencher

1. Introduction

Adenosine triphosphate (ATP) as a universal energy currency in biological organisms holds a pivotal role in adjusting cellular metabolizability pathways and various biochemical reaction processes.[1-3] The abnormalities of ATP content prompts the occurrences of cell viability, injury, necrosis and apoptosis, which could further induce certain diseases such as malignant tumors, angiocardiopathy, Alzheimer's and Parkinson's diseases.[4, 5] Plenty of evidences demonstrate that ATP has been acknowledged as a powerful and reliable indicator for the diagnosis of disease,

monitoring of disease progression and evaluation of prognosis.[6, 7] Considering the great significance of ATP in clinical applications, it is urgent to develop an accurate, specific and ultrasensitive approach to detect ATP. Although various analysis methods, including chemiluminescence, fluorescence, electrochemiluminescence, electrochemistry and colorimetry, have been implemented for ATP detection, the background signal and stability of these methods should be improved furtherly to satisfy the demand of ultrasensitive ATP determination.[8-12] Currently, photoelectrochemical (PEC) assay as an emerging and developing analytical technique has attracted intense attention due to its low background signal, excellent stability and ultra-high sensitivity, which has been extensively applied in ultrasensitive detection of various targets.[13, 14] In view of these merits, PEC assay might be a promising analysis method for developing a highly sensitive and accurate ATP detection strategy.

The PEC process refers to the photon-electricity conversion, which originates from the electron excitation and following charge transfer of photoactive materials under illumination.[15] As a classic signal mode for PEC sensing, the "signal-off" mode has been applied in a broad range for its intrinsic virtues of simple structure, convenient operation and good stability.[16] An ideal photoactive material with desirable PEC signal and an efficient quencher with significant quenching effect are essential requirements to construct a "signal-off" PEC sensing. Recent years, with the rise of carbon nanomaterials, fullerene (C_{60}) has gained extensive attention in the PEC

field for its excellent photovoltaic properties.[17, 18] Deepa's group reported a quantum dot solar cell based on the TiO_2/CdS/CdSeS/C_{60}/Au@poly(acrylic acid) photoanode matrix that showed high photo-current conversion efficiency.[17] Hu's group reported an all-carbon PEC immunosensing protocol for ultrasensitive target detection by using carboxylated multi-wall carbon nanotube-Congo red-C_{60} nanohybrids as a signal probe.[18] Although photovoltaic performances of the above devices demonstrated prominent improvements, there are still several drawbacks including complicated preparation procedure and cockamamie modification process. Therefore, there is a real need for developing a simple and highly efficient approach for applying C_{60} in the PEC field. MoS_2, a classic transition metal chalcogenide with S-Mo-S trip atomic layers, exhibits excellent intrinsic conductivity and unique optical property. In particular, the 1.9 eV band gap of MoS_2 matches well with that of 2.6 eV of C_{60}, making MoS_2 an ideal candidate for enhancing the PEC signal of C_{60}.[19-21] Accordingly, we have synthesized a novel C_{60} decorated Au nanoparticle@MoS_2 (C_{60}-Au NP@MoS_2) composite material with desirable PEC signal by combining -SH functionalized C_{60} and Au nanoparticle@MoS_2 (Au NP@MoS_2), which is expected to enhance the loading of C_{60} as well as simplify the preparation and modification processes.

Another major aspect of our work lies in identifying an efficient quencher with significant quenching effect to develop an approving "signal-off" PEC sensing. Currently, the p-n type quenching has become one of the most effective quenching

modes in PEC system, which is attributed to the fact that p-type semiconductor could compete with n-type semiconductor to consume light energy and electron donor, resulting in the significant quenching effect of p-type semiconductor towards n-type semiconductor. Recently, Zhu's group reported a p-n type quenching strategy that selected p-type CuS nanocrystals as a quencher of n-type TiO_2/CdSeTe@CdS:Mn composite structure for ultrasensitive biomarker detection.[22] However, the quenching efficiency of CuS nanocrystals is still limited due to the weak light absorption capacity caused by its wide band gap (2.0 eV). Therefore, a p-type semiconductor with narrower band gap and stronger light absorption capacity is necessary. P-type PbS quantum dots (PbS QDs) possesses a narrower band gap value (1.17 eV) than that of CuS nanocrystals, which is an ideal quenching candidate for strengthening light absorption capacity and improving quenching efficiency.[23, 24] Given these advantages, in the present work, p-type PbS QDs were used as an efficient quencher towards n-type C_{60}-Au NP@MoS_2 composite material. Meanwhile, the experimental results demonstrate that the p-type PbS QDs exhibited higher quenching efficiency compared with the CuS nanocrystals.

Herein, a novel "signal-off" PEC biosensor for ultrasensitive ATP detection was proposed by using an n-type C_{60}-Au NP@MoS_2 composite material as a signal indicator and a p-type PbS QD as an efficient signal quencher, which was depicted in Scheme 1. The n-type C_{60}-Au NP@MoS_2 composite material was synthesized by coupling the photoactive material C_{60} and its signal enhancer (MoS_2). The

combination of wide band gap C_{60} and narrow band gap MoS_2 could promote charge separation, reduce the electron-hole recombination and improve photocurrent conversion efficiency, which could achieve a desirable PEC signal. Besides, the target mediated aptazyme cycling amplification strategy not only can recognize target with high affinity and specificity, but also can catalyze multiple-turnover reactions for signal amplification. In this work, the target mediated aptazyme cycling amplification strategy was adopted, which could convert a limited amount of ATP into numerous PbS QD-labeled short DNA sequences (output S_1) though cyclic cleaving of aptazyme at the cleavage sites, leading to effective target signal conversion and amplification. Thereafter, these cleaved output S_1 could hybridize with the capture DNA on the C_{60}-Au NP@MoS_2 modified electrode surface to availably quench PEC signal of C_{60}-Au NP@MoS_2, which were ascribed to some key reasons: the p-type PbS QDs competed with C_{60}-Au NP@MoS_2 to absorb light energy and capture electron donor and the electron transfer was retarded owing to the steric hindrance of PbS QDs. The decreased PEC signal is quantitatively correlated with the magnitude of the output S_1, which is related to the concentration of ATP. The successful establishment of this "signal-off" PEC biosensor for ultrasensitive ATP detection revealed a new horizon for the clinical applications of ATP-related diseases, including diagnosis of disease, monitoring of disease progression and evaluation of prognosis.

2. Experimental

2.1 Chemicals and apparatus

Hexanethiol (HT), mercaptohexanol (MCH) and gold chloride tetrahydrate ($HAuCl_4 \cdot 4H_2O$) were bought from Sigma-Aldrich (St. Louis. MO, USA). ATP, uridine triphosphate (UTP), cytidine triphosphate (CTP) and guanosine triphosphate (GTP) were bought from Worthington Biochemicals (Lakewood, NJ, USA). Thioglycolic acid (TGA) was purchased from Xiya Reagent Ltd. (Chengdu, China). L-cysteine and C_{60} were bought from J&K Scientific Ltd. (Beijing, China). Amido-modified Fe_3O_4 (Fe_3O_4-NH_2) magnetic microspheres were purchased from Tianjin BaseLine Chrom Tech Research Centre (Tianjin, China). $K_3[Fe(CN)_6]$ and $K_4[Fe(CN)_6]$ were obtained from Beijing Chemical Reagent Co. (Beijing, China). N-(3-dimethylaminopropyl)-N′-ethylcarbodiimide hydrochloride (EDC) and N-hydroxy succinimide (NHS) were supplied by Shanghai Medpep Co., Ltd. (Shanghai, China). Ascorbic acid (AA) was bought from Sinopharm Chemical Reagent Co., Ltd. (Shanghai, China). Sodium sulfide nonahydrate ($Na_2S \cdot 9H_2O$), sodiummolybdate dihydrate ($Na_2MoO_4 \cdot 2H_2O$) were obtained from Chengdu KeLong Co., Ltd. (Chengdu, China). Lead nitrate ($Pb(NO_3)_2$) was obtained from Tianjin Guangfu Fine Chemical Research Institute (Tianjin, China). In our work, 0.1 M phosphate buffered saline (PBS, pH 7.0) was prepared using 0.1 M KH_2PO_4, 0.1 M KCl and 0.1 M Na_2HPO_4. Other chemicals were of analytical grade and used throughout this work without further purification. Ultrapure water was employed for preparing solutions in this work. The oligonucleotides sequences were ordered from Sangon Inc. (Shanghai, China), which are listed as follows:

Capture DNA: 5′-CAT CTC TTC CCC CCC-SH-3′

DNA linker: 5′-SH-AAA AAA AAA ATT CAC CAA CTA TrA GGA AGA GAT GAA AA-NH_2-3′

Aptazyme strand: 5′-CAT CTC TTC AGC GAT CTA GGG GGA GTA TTG CGG AGG ATA GCA CCC ATG TTA GTT GGT GAA-3′

2.2. Apparatus and measurements

PEC measurements were performed using a PEC workstation (Ivium, Netherlands) connected to a three-electrode system consisting of a platinum wire counter electrode, an Ag/AgCl (saturated KCl) reference electrode and a glassy carbon working electrode (GCE, Φ = 4 mm). Cyclic voltammetric (CV) and electrochemical impedance spectroscopy (EIS) measurements were carried out on a CHI 660e electrochemistry workstation (Shanghai Chenhua Instrumission, China). UV-vis absorption spectroscopy was performed using a UV-2450 UV-vis spectrophotometer (Shimadzu, Tokyo, Japan). The morphologies of the prepared nanomaterials were obtained from three kinds of scanning electron microscopes (Hitachi S-4800 microscope at voltage of 30 kV, JEOL JSM-7800F microscope at voltage of 5 kV and FEI Nova NanoSEM450 at voltage of 1 kV).

2.3 Synthesis of C_{60} NPs and Au NP@MoS_2

C_{60} NPs were prepared as described by us previously.[25] Flower-like MoS_2 was prepared according to the literature with slight modifications.[26] Briefly, 0.31 g $Na_2MoO_4 \cdot 2H_2O$ was added to 30 mL ultrapure water, followed by dropwise addition of 12 M HCl for adjusting the pH to 6.5. Subsequently, 5 mL of freshly prepared

aqueous L-cysteine solution (1.35 M) was added under gentle stirring for 1 h. After that, the mixture reacted in a 50 mL Teflon-lined stainless steel autoclave at 180 ℃ for 48 h. Finally, the obtained flower-like MoS_2 was centrifugally washed three times with ethanol and ultrapure water, respectively. The product was dispersed in 30 mL ultrapure water for further use. Based on flower-like MoS_2, the Au NP@MoS_2 was prepared through *in situ* growth of Au NPs on flower-like MoS_2 *via* a cysteine-linking strategy, which followed the method reported in Cao's group.[27] Initially, 2 mL flower-like MoS_2 aqueous solutions was mixed with 5 mL L-cysteine aqueous solution (1 mM) with continual ultrasonication for 30 min. Subsequently, 5 mL $HAuCl_4$ aqueous solution (0.3 mM) was introduced into above mixture solution under vigorous stirring for 30 min. After that, 10 mL AA aqueous solution (5 mM) was added as quickly as possible, followed by stirring rapidly for 3 h. Finally, Au NP@MoS_2 was collected by centrifugation and washing with ultrapure water several times.

2.4 Synthesis of C_{60}-Au NP@MoS_2

The overall synthetic process of C_{60}-Au NP@MoS_2 was shown schematically in Figure S2 (Supporting Information). The C_{60}-Au NP@MoS_2 was prepared through the special interaction between Au NP@MoS_2 and -SH functionalized C_{60} NPs.[25] Briefly, 2 mL of the synthesized Au NP@MoS_2 was added into 3 mL the as-prepared C_{60} NPs while stirring. After being stirred overnight at room temperature, the resultant C_{60}-Au

NP@MoS_2 was centrifuged and washed to remove unreacted reagents. Finally, the obtained C_{60}-Au NP@MoS_2 was redispersed in 1 mL ultrapure water.

2.5 Synthesis of Au@Fe_3O_4 and PbS QD-labeled DNA linker

Au@Fe_3O_4 was prepared in accordance with our previous report.[28] The TGA-capped PbS QDs were prepared under a highly pure nitrogen-filled atmosphere through an established protocol.[23] Briefly, 10 μL the as-prepared TGA-capped PbS QDs were mixed with 20 μL coupling reagent (20 mM EDC and 10 mM NHS) at room temperature for 1 h for activating -COOH groups of TGA-capped PbS QDs. After centrifugation, 30 μL 4 μM DNA linker was added to the activated PbS QDs for 1 h, which would covalently couple to the DNA linker on the surface of PbS QDs *via* a classic acylation reaction.

2.6 ATP mediated aptazyme cycling amplification procedure

The ATP mediated aptazyme cycling amplification procedure was performed in an eppendorf tube according to an established protocol with minor modifications,[29, 30] which was shown schematically in Scheme 1(A). Briefly, 90 μL the as-prepared Au@Fe_3O_4 and 30 μL PbS QD-labelled DNA linker were mixed and reacted for 12 h. Thus the PbS QD-labelled DNA linker was assembled on the surface of Au@Fe_3O_4 *via* Au-S bond for further magnetic separation. In order to block the nonspecific sites, the above solution was incubated with 20 μL 1 mM HT for 40 min. Subsequently, 10 μL 4 μM aptazyme strand (containing ATP aptamer sequence and Mg^{2+}-dependent

DNAzyme sequence) was added. The obtained mixture was heated to 85 °C for 10 min, before it was slowly cooled to room temperature. This mixture was then stored in the dark for 12 h to complete the hybridization between the PbS QD-labelled DNA linker and aptazyme strand. After incubation in 20 μL ATP with different concentrations at room temperature for 90 min, a hairpin structure for aptamer domain-ATP was formed, which was used to activate the Mg^{2+}-dependent aptazyme strand. Finally, 10 μL of 360 mM aqueous Mg^{2+} solution was added and incubated for 80 min to obtain a final concentration of 20 mM for Mg^{2+}. In the presence of both the target ATP and the cofactor Mg^{2+}, the activated aptazyme would cleave the PbS QD-labelled DNA linker, generating numerous output S_1. After magnetic separation, the supernatant containing plenty of output S_1 was applied to the modified electrode for PEC measurements.

2.7 Construction of PEC biosensor

The construction procedure and the function of a PEC biosensor are illustrated in Scheme 1. Prior to modification, the GCE was carefully polished with α-Al_2O_3 powders (0.3, 0.05 μm), followed by ultrasonic cleaning in ultrapure water and drying with nitrogen. Then, the mirror-like GCE was modified with the as-prepared C_{60}-Au NP@MoS_2 (15 μL) and dried at 37 °C for forming a homogeneous film. Subsequently, 15 μL 4 μM thiol-modified capture DNA was attached on the C_{60}-Au NP@MoS_2 layer and incubated at room temperature for 12 h, leading to immobilization of capture DNA on the modified electrode *via* Au-S bond. After

blocking with 1 mM MCH for 1 h, the obtained electrode was incubated with 20 μL output S_1 at 37 °C for 2 h to hybridize with the capture DNA on the electrode. After each modification, the electrode was thoroughly washed with ultrapure water to remove physically absorbed species.

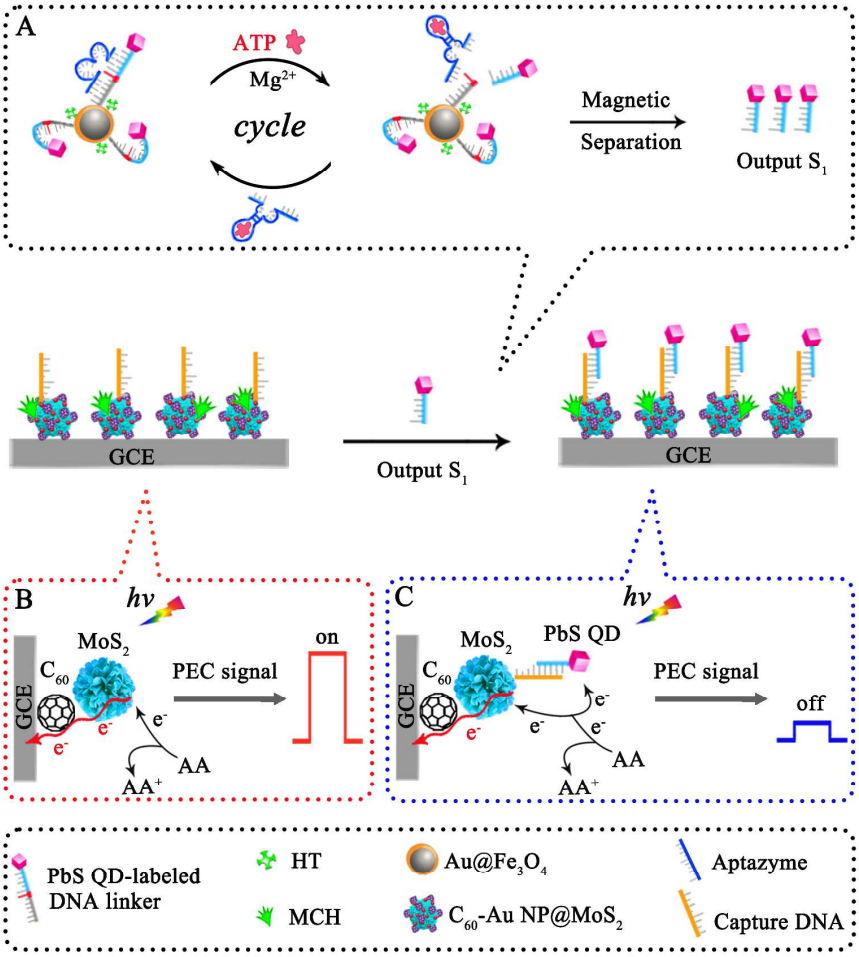

Scheme 1. Schematic illustrations of the PEC biosensor for ATP detection. (A) ATP mediated aptazyme cycling amplification procedure. Schematic illustrations of the photocurrent generating (B) and quenching (C) mechanism.

2.8 PEC measurement

The PEC biosensor was investigated in 5 mL PBS containing 0.1 M freshly prepared AA solution at room temperature. As illustrated in Figure 4, AA was an effective electron donor for hole-scavenging in the photoexcited photoactive materials, which could promote the separation of electron-hole and suppress the electron-hole recombination, achieving the generation of a stable photocurrent. The excitation light source (wavelength: λ = 460 nm; radiant flux: Φ = 976 mW) was provided by a LED lamp and switched off-on-off for 10 s-20 s-10 s under 0.0 V potential.

3. Results and discussions

3.1 Characterization of the different nanomaterials

The morphologies of prepared nanomaterials were characterized by scanning electron microscopy and transmission electron microscopy (TEM). As shown in Figure 1A, the as-prepared C_{60} NPs exhibited globular structures with the size about 80 nm (with a standard deviation of 25 nm; N = 148). The obtained MoS_2 presented a flower-like shape with a uniform diameter of 400 nm, which was shown in Figure 1B. After cysteine-linking of Au NPs, the average size increased by ~50% on the surface of flower-like MoS_2 (Figure 1C). After reacting with the synthesized C_{60} NPs, numerous globular structures were obviously observed on the Au NP@MoS_2 surface (Figure 1D and Figure 1E). Moreover, a typical transmission electron micrograph (Figure 1F) revealed that the synthesized PbS QDs possessed homogeneous

dispersion and clear lattice planes with the average size about 4 nm. These results indicated the successful formation of C_{60} NPs, MoS_2, Au NP@MoS_2, C_{60}-Au NP@MoS_2 and PbS QDs. Besides, scanning electron micrograph of Au@Fe_3O_4 was shown in Figure S3 (Supporting Information).

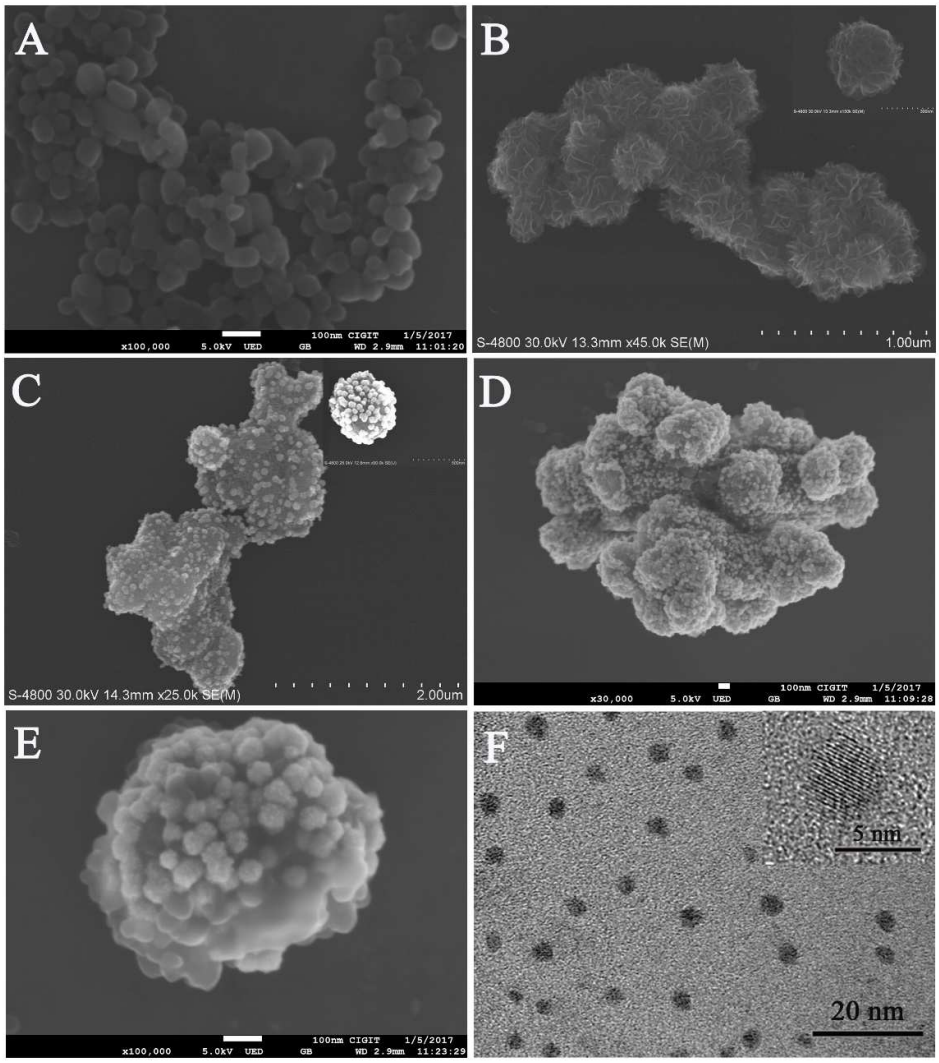

Figure 1. Scanning electron micrographs of C_{60} NPs (A), MoS_2 (B), Au NP@MoS_2 (C), and C_{60}-Au NP@MoS_2 (D and E), and TEM images of PbS QDs (F). The inserts of (B) and (C) showed an individually enlarged scanning electron micrographs of

MoS_2 and Au NP@MoS_2, respectively. The insert of (F) showed a high-resolution TEM image of PbS QDs.

The scanning electron micrographs confirmed that the synthesized C_{60} NPs with -SH functionalization have been attached to the Au-S-Mo nanostructure via the interaction between Au NPs and -SH groups (Figure 2A). In addition, UV-vis absorption spectroscopy was performed to further examine the successful preparation of MoS_2, Au NPs, Au NP@MoS_2, C_{60} NPs and C_{60}-Au NP@MoS_2. As displayed in Figure 2B, the characteristic absorption peaks of MoS_2 alone (curve a) were observed around 208 nm and 230 nm, which was consistent with the reported absorption peaks in the near-UV region (λ < 300 nm).[31, 32] The result might be attributable to the excitonic features of MoS_2.[20, 31] Au NPs had a strong characteristic absorption peak at 520 nm (curve b), which originates from its localized surface plasmon resonance.[33, 34] Au NP@MoS_2 (curve c) exhibited two weak absorption peaks around 208 nm and 230 nm due to the excitonic features of MoS_2.[20, 31] Meanwhile, a wide absorption peak around 385 nm was also obtained in curve c, owing to the contribution of the oxidized states of gold.[35, 36] Because of the dipole-allowed transitions in C_{60}, the spectrum of C_{60} NPs (curve d) displayed three clear characteristic absorption peaks at 218 nm, 262 nm and 337 nm, respectively.[25] Comparing with C_{60} NPs, the characteristic absorption peaks of C_{60}-Au NP@MoS_2 (curve e) presented obvious red shifts (about 10 nm). These results demonstrated the successful preparation of MoS_2, Au NPs, Au NP@MoS_2, C_{60} NPs and C_{60}-Au NP@MoS_2.

Furthermore, X-ray photoelectron spectroscopy (XPS) was employed for the elemental analysis to prove the successful synthesis of C_{60}-Au NP@MoS_2 composite material. As seen from Figure 2C, the peaks at 284.8, 400 and 532 eV might be assigned to C1s, N1s and O1s, respectively, which is consistent with some literatures and suggests the presence of C, N, O elements.[37-39] Besides, the doublets at 228.8 and 232 eV belonged to Mo3d, and the peaks located at 163.6 and 168 eV was corresponding to S2p, which indicated the presence of Mo, S elements.[21, 26, 40] Additionally, the XPS characteristic peaks for Au4f (84 and 87.7 eV) proved the existence of Au element.[40-42] The elemental analysis results verified that the C_{60}-Au NP@MoS_2 composite material might be successfully prepared.

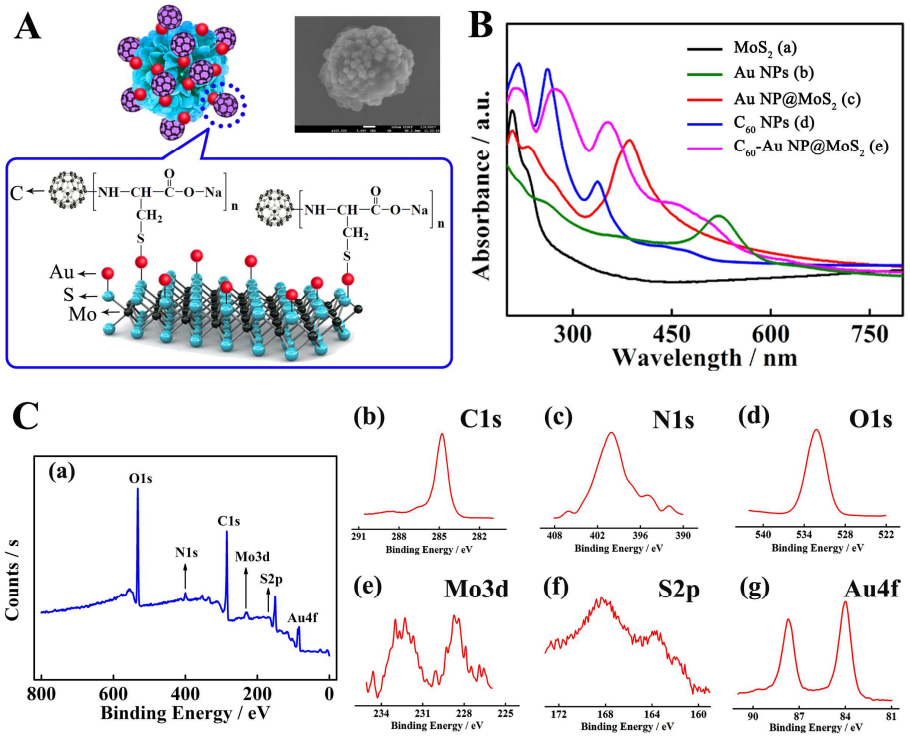

Figure 2. (A) Schematic diagrams of the structure and morphology for C_{60}-Au NP@MoS_2. (B) UV-vis adsorption spectrums of (a) MoS_2, (b) Au NPs, (c) Au NP@MoS_2, (d) C_{60} NPs and (e) C_{60}-Au NP@MoS_2. (C) XPS analysis for (a) the full region of C_{60}-Au NP@MoS_2, (b) C1s region, (c) N1s region, (d) O1s region, (e) Mo3d region, (f) S2p region and (g) Au4f region.

3.2 Comparison of PEC responses for different nanomaterials

To confirm the superiority of C_{60}-Au NP@MoS_2 as a photoactive material, two components including Au NP@MoS_2 and C_{60} NPs were utilized as controls. The comparison study concerning these nanomaterials was conducted under the same experimental conditions, and the results obtained are shown in Figure 3. The photocurrent responses of Au NP@MoS_2 (Figure 3A) and C_{60} NPs (Figure 3B) were 0.48 μA and 0.9 μA, respectively. For the C_{60}-Au NP@MoS_2 modified GCE (Figure 3C), the observed photocurrent response (1.9 μA) was about 2-fold higher than that of C_{60} NPs, which was attributed to the enhancement effect of MoS_2 towards C_{60} NPs. These comparison results indicated that C_{60}-Au NP@MoS_2 could be employed as a preferable photoactive material for construction of PEC biosensor.

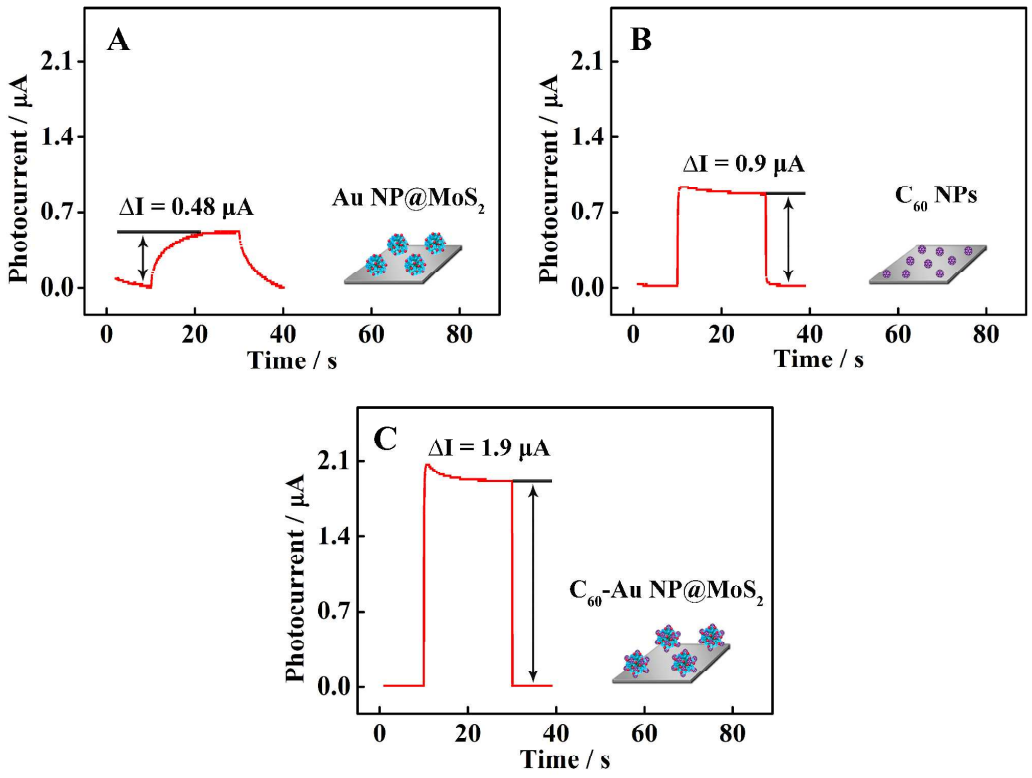

Figure 3. PEC responses of different nanomaterials: (A) Au NP@MoS_2, (B) C_{60} NPs and (C) C_{60}-Au NP@MoS_2. The PEC measurements were performed in 5 mL PBS (pH 7.0, 0.1 M) containing 0.1 M AA.

3.3 PEC mechanism of the biosensor

The photocurrent generating and quenching mechanisms of this PEC biosensor are illustrated in Figure 4A and Figure 4B, respectively. C_{60} is an excellent photoactive material in PEC sensing field because of its generally recognized photovoltaic properties such as strong electron-accepting capacity and predominant electronic absorption bands throughout the entire UV-vis spectrum.[18, 43] Nevertheless, the existence of its wide band gap (2.6 eV) has led to limited photo-current conversion

efficiency.[44] In developing an ultrasensitive assay, it is essential to improve the photocurrent response of C_{60}. In this regard, coupling wide band gap C_{60} with narrow band gap semiconductor is highly promising, which will promote charge separation, raise the utilization of light energy and reduce the electron-hole recombination, leading to a significantly enhanced photocurrent response.[45, 46] Compared with C_{60}, MoS_2 possesses a narrower band gap (1.9 eV), which is beneficial for injecting photogenerated electrons from MoS_2 to C_{60} and improving photocurrent conversion efficiency.[19, 20] Hence, as shown in Figure 4A, a novel C_{60}-Au NP@MoS_2 composite structure was synthesized that selected C_{60} as photoactive material and MoS_2 as PEC signal enhancer to obtain a desirable initial amplified photocurrent response.

Besides, as a signal quenching element, the p-type PbS QDs were introduced through DNA hybridization, which could effectively quench the photocurrent response of C_{60}-Au NP@MoS_2.[22] First, the p-type PbS QDs competed with C_{60}-Au NP@MoS_2 to absorb light energy due to their broad absorption spectrum, which could weaken the light absorption of C_{60}-Au NP@MoS_2, leading to decreased photocurrent response.[23] Second, the photogenerated electrons of PbS QDs were captured by dissolved oxygen (electron acceptors) to form $O_2^{-\bullet}$ (e), and the photogenerated holes were neutralized with AA (d), which could reduce AA concentration supplied for C_{60}-Au NP@MoS_2, making the photocurrent response decrease further. Third, the electron transfer was retarded owing to the steric hindrance of PbS QDs, which could also reduce the photocurrent response. Herein, an effectively quenched photocurrent

response was obtained in the presence of the quencher p-type PbS QDs, which was shown in Figure 4B.

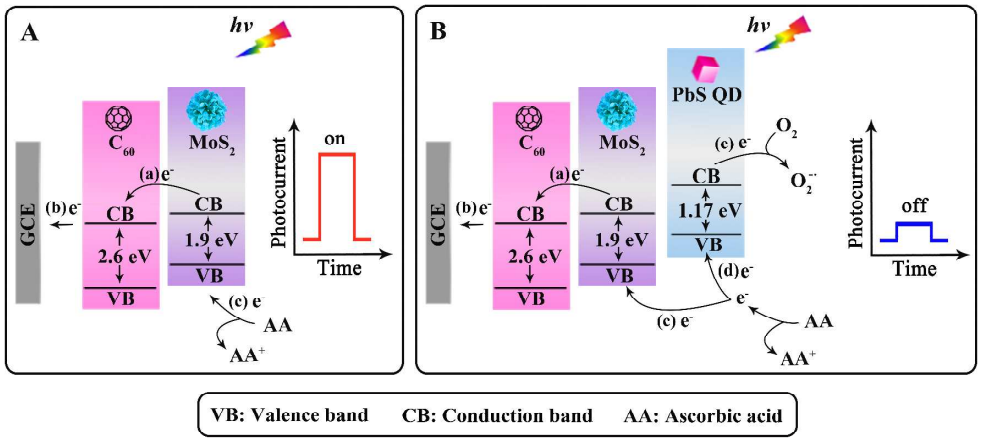

Figure 4. Schematic illustration of (A) the photocurrent generating mechanism of C_{60} NPs/MoS_2 photoactive materials and (B) the photocurrent quenching mechanism of p-type PbS QDs towards C_{60} NPs/MoS_2 photoactive materials.

3.4 PEC characterization of the biosensor

The photocurrent characterization of the stepwise-modified procedure for the proposed PEC biosensor is shown in Figure 5. After C_{60}-Au NP@MoS_2 was coated onto the pretreated bare GCE, the photocurrent enhanced greatly (curve b) compared to that of the bare GCE (curve a), which was ascribed to the excellent photoelectric activity of C_{60}-Au NP@MoS_2. Subsequent incubating with capture DNA caused obvious inhibition of the photocurrent (curve c) and the inhibition percentage from curve b to curve c was 6.83%, owing to the poor charge transfer of DNA skeleton. As expected, a further decreased photocurrent (curve d) was recorded and the reduction

percentage from curve c to curve d was 13.59% after blocking with the organic small molecule MCH. Finally, a significant depression of the photocurrent was appeared (curve e) and the reduction percentage from curve d to curve e was 60.84% when output S_1 was modified on the above electrode, because output S_1 was successfully captured in which the p-type PbS QDs could effectively quench the photocurrent of C_{60}-Au NP@MoS_2 composite material and the maximum quenching percentage reached about 74%. Zhu's group has reported that the maximum quenching percentage of p-type CuS nanocrystals is 66.67%.[22] The result demonstrates that the p-type PbS QDs has higher quenching efficiency compared with the CuS nanocrystals, which are ascribed to the p-type PbS QDs with narrower band gap and stronger light absorption capacity.

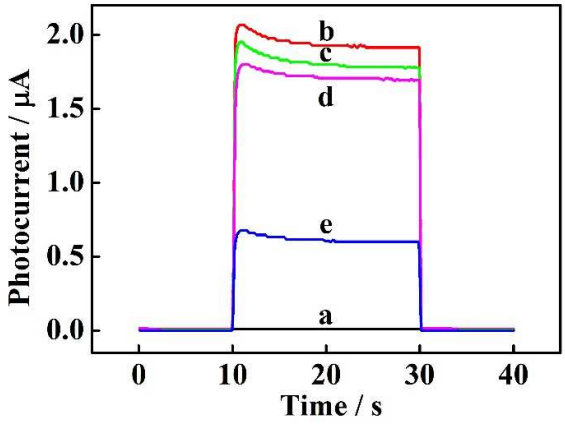

Figure 5. PEC responses of (a) bare GCE, (b) C_{60}-Au NP@MoS_2/GCE, (c) capture DNA/C_{60}-Au NP@MoS_2/GCE, (d) MCH/capture DNA/C_{60}-Au NP@MoS_2/GCE and (e) output S_1/MCH/capture DNA/C_{60}-Au NP@MoS_2/GCE. The PEC measurements were performed in 5 mL PBS (pH 7.0, 0.1 M) containing 0.1 M AA.

3.5 Electrochemical characterizations of the PEC biosensor

To characterize the PEC biosensor preparation procedure step by step, CV measurements were conducted in 2 mL PBS (pH 7.0, 0.1 M) containing 5.0 mM $[Fe(CN)_6]^{3-/4-}$ and 0.1 M KCl between -0.2 V and 0.6 V at a scan rate of 50 mV/s. As displayed in Figure 6A, the bare GCE (curve a) exhibited a pair of reversible redox peaks and the oxidation peak current was obtained as 232.3 μA. With C_{60}-Au NP@MoS_2 coated onto the electrode surface, the oxidation peak current decreased to 213.4 μA (curve b) because of the poor conductivity of C_{60}-Au NP@MoS_2. The introduction of capture DNA induced further decrease of the peak current (curve c) and the oxidation peak current was obtained as 178.2 μA, owing to the electronic repulsion between $[Fe(CN)_6]^{3-/4-}$ and the negatively charged capture DNA. The observed oxidation peak current (160.3 μA) decreased once again (curve d) after blocking with MCH. Finally, when PbS QD-labeled short DNA sequences (output S_1) was immobilized onto the above electrode, the obtained oxidation peak current decreased to 152.3 μA (curve e) which attributed to the increased steric hindrance effect and electronic repulsion.

Meanwhile, as shown in Figure 6B, EIS measurements were employed to characterize the fabrication of PEC biosensor. EIS measurements were recorded in 2 mL PBS (pH 7.0, 0.1 M) containing 5.0 mM $[Fe(CN)_6]^{3-/4-}$ and 0.1 M KCl, which was conducted over a frequency range from 10 kHz to 0.1 Hz using an AC potential with an amplitude of 5 mV at a DC potential of 0.22 V. The charge-transfer resistance (R_{et})

for bare GCE was about 24 Ω (curve a). Comparing with curve a, an increased R_{et} was observed for the C_{60}-Au NP@MoS_2 modified electrode (R_{et} ≈ 112 Ω, curve b). The R_{et} increased sequentially with the consecutive assembling of negatively charged capture DNA (R_{et} ≈ 332 Ω, curve c) and nonconductive MCH (R_{et} ≈ 416 Ω, curve d). A further increase of the R_{et} was found after incubating with output S_1 (R_{et} ≈ 562 Ω, curve e) because of the largely increased negative charges as well as the increased steric hindrance effect. Give the hint that the PEC biosensor has been successfully fabricated.

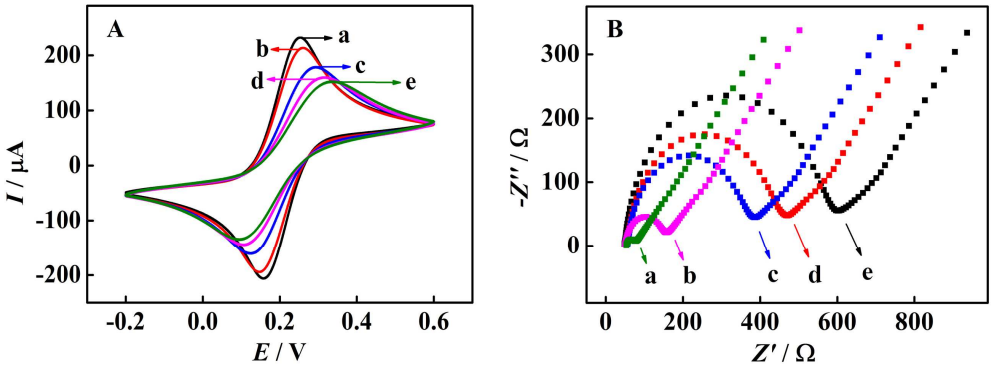

Figure 6. CV (A) and EIS (B) responses of the stepwise modified electrodes: (a) bare GCE, (b) C_{60}-Au NP@MoS_2/GCE, (c) capture DNA/C_{60}-Au NP@MoS_2/GCE, (d) MCH/capture DNA/C_{60}-Au NP@MoS_2/GCE and (e) output S_1/MCH/capture DNA/C_{60}-Au NP@MoS_2/GCE.

3.6 PEC analysis of ATP at the developed biosensor

To investigate the analytical performance of the PEC biosensor, the quantitative measurement was explored by detecting ATP with various concentrations under the

optimal experiment conditions (Supporting Information, Figure S1). As depicted in Figure 7, the PEC response linearly decreased with incremental ATP concentration from 1.00×10^{-2} pM to 100 nM with a detection limit of 3.30 fM (defined as LOD = $3S_B/m$, where S_B and m were the standard deviation of the blank and the slope of the calibration plot at lower concentration ranges, respectively), and the linear regression equation expressed as $I = -0.145 \lg c + 0.776$ with a correlation coefficient of 0.995 (where I and c were the PEC response and the ATP concentration, respectively). Additionally, the analytical performances of the proposed PEC biosensor were compared with some previously reported methods for ATP detection. As seen from Table S1 (Supporting Information), an improved sensitivity and a much wider linear range were observed in our work. These results demonstrated that the proposal PEC biosensor possessed excellent potential for ultrasensitive detection of ATP.

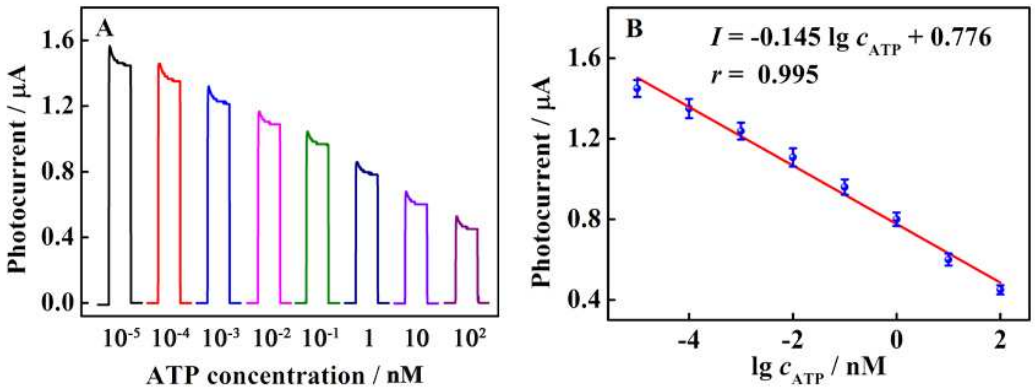

Figure 7. (A) PEC responses of the biosensor in the presence of ATP with various concentrations: 1.00×10^{-2} pM, 1.00×10^{-1} pM, 1.00 pM, 1.00×10^{-2} nM, 1.00×10^{-1}

nM, 1.00 nM, 10.0 nM and 100 nM (from left to right). (B) The corresponding calibration curve for ATP detection.

3.7 Selectivity and stability of the PEC biosensor

To explore the selectivity of the PEC biosensor, several possible interfering agents including UTP, CTP and GTP were assessed as controls. As shown in Figure 8A, the PEC response of the blank test exhibited no difference in comparison with 10 μM GTP, 10 μM UTP and 10 μM CTP. However, a significant decreased PEC response was achieved when 100 nM ATP was served as the detection sample. Meanwhile, the mixture containing 10 μM GTP, 10 μM UTP, 10 μM CTP and 100 nM ATP exhibited no obvious change in PEC response compared with the case of solely ATP. The result suggested a good selectivity of the proposal PEC biosensor for ATP assay. Furthermore, the proposal PEC biosensor incubated with 0.1 nM ATP was monitored under successive periodic "off-on-off" light for 10 cycles to investigate the stability of this strategy. As illustrated in Figure 8B, the relative standard deviation (RSD) for PEC responses was 3.22%, which indicated an excellent stability of the proposal PEC biosensor for ATP detection.

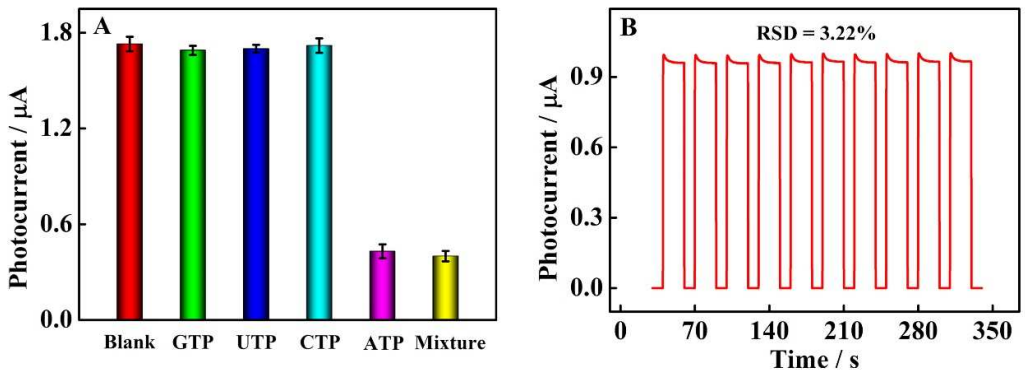

Figure 8. (A) Selectivity of the PEC biosensor with different targets: 10 μM GTP, 10 μM UTP, 10 μM CTP, 100 nM ATP and the mixture containing 10 μM GTP, 10 μM UTP, 10 μM CTP and 100 nM ATP. (B) Stability of the PEC biosensor in the presence of 0.1 nM ATP under periodic "off-on-off" light for 10 cycles.

3.8 Preliminary application in human serum samples for ATP detection

The recovery experiment of the PEC biosensor was conducted by detecting ATP in real-life human serum samples for evaluating the feasibility of this strategy. Briefly, the healthy human real serum samples (provided by Ninth People's Hospital of Chongqing, China) was diluted 50-fold and utilized to prepare different concentrations of ATP for further detection. As tabulated in Table 1, the recovery ranged from 93.16% to 108.50%, which indicated the excellent potentiality of this strategy for ATP determination in real biological samples.

Table 1. Determination of ATP added in human serum samples with the proposed PEC biosensor.

Sample number	Added / (nM)	Found / (nM)	Recovery / %
1	50.00	46.58	93.16
2	2.00	2.17	108.50
3	5.00×10^{-2}	5.05×10^{-2}	101.00
4	1.00×10^{-3}	0.96×10^{-3}	96.00
5	5.00×10^{-5}	4.74×10^{-5}	94.80

4. Conclusion

In summary, this work developed a novel "signal-off" PEC strategy by using an n-type C_{60}-Au NP@MoS_2 composite material as a signal indicator and a p-type PbS QD as an efficient signal quencher for ultrasensitive detection of ATP. The synthesized C_{60}-Au NP@MoS_2 composite material with superior photovoltaic properties presented nearly 2-fold higher photocurrent response than that of C_{60} due to the enhancement effect of C_{60} by MoS_2. Moreover, using a p-type PbS QD as a signal quencher, the photocurrent response of C_{60}-Au NP@MoS_2 was effectively quenched, which was attributed to the significant quenching effect of p-type PbS QDs towards n-type C_{60}-Au NP@MoS_2. With the aid of target mediated aptazyme cycling amplification strategy, the conversion of a limited amount of ATP into an amplified output S_1 was achieved, and these PbS QD-labeled output S_1 were obtained to amplify the quenching effect furthermore. By combining the C_{60}-AuNP@MoS_2 composite material and the efficient quencher p-type PbS QDs, our proposed strategy showed a higher sensitivity and a much wider linear range compared with previously reported methods for ATP detection. In view of these results, the developed "signal-off" PEC strategy provides a modular platform for ATP ultrasensitive detection and paves a

new avenue in clinical applications of ATP-related diseases, including diagnosis of disease, monitoring of disease progression and evaluation of prognosis.

ASSOCIATED CONTENT

Supporting Information

Condition optimization (Figure S1), the synthesis of C_{60}-Au NP@MoS_2 (Figure S2), characterization of Au@Fe_3O_4 (Figure S3), PEC analysis of ATP at the developed biosensor (Figure S4) and comparisons of the ATP detection with other detection methods (Table S1) were supplied in Supporting Information.

AUTHOR INFORMATION

* Corresponding authors:

Tel.: +86-23-68252277; Fax: +86-23-68253172.

E-mail address: yuanruo@swu.edu.cn (R. Yuan), yqchai@swu.edu.cn (Y. Q. Chai)

ACKNOLEDGEMENT

This work was financially supported by the NNSF of China (21675129, 51473136, 21575116) and the Fundamental Research Funds for the Central Universities (XDJK2015A002), China.

REFERENCES

1. Deng, J. J.; Wang, K.; Wang, M.; Yu, P.; Mao, L. Q. Mitochondria Targeted Nanoscale Zeolitic Imidazole Framework-90 for ATP Imaging in Live Cells. *J. Am. Chem. Soc.* **2017**, *139*, 5877-5882.
2. Lu, L. M.; Zhang, X. B.; Kong, R. M.; Yang, B.; Tan, W. H. A Ligation-Triggered

DNAzyme Cascade for Amplified Fluorescence Detection of Biological Small Molecules with Zero-Background Signal. *J. Am. Chem. Soc.* **2011**, *133*, 11686-11691.

3. Zhang, Y. J.; Clausmeyer, J.; Babakinejad, B.; Córdoba, A. L.; Ali, T.; Shevchuk, A.; Takahashi, Y.; Novak, P.; Edwards, C.; Lab, M.; Gopal, S.; Chiappini, C.; Anand, U.; Magnani, L.; Coombes, R. C.; Gorelik, J.; Matsue, T.; Schuhmann, W.; Klenerman, D.; Sviderskaya, E. V.; Korchev, Y. Spearhead Nanometric Field-Effect Transistor Sensors for Single-Cell Analysis. *ACS Nano* **2016**, *10*, 3214-3221.
4. Lin, C. S.; Cai, Z. X.; Wang, Y. R.; Zhu, Z.; Yang, C. Y. J.; Chen, X. Label-Free Fluorescence Strategy for Sensitive Detection of Adenosine Triphosphate Using a Loop DNA Probe with Low Background Noise. *Anal. Chem.* **2014**, *86*, 6758-6762.
5. Li, X.; Peng, Y.; Chai, Y. Q.; Yuan, R.; Xiang, Y. A Target Responsive Aptamer Machine for Label-Free and Sensitive Non-Enzymatic Recycling Amplification Detection of ATP. *Chem. Commun.* **2016**, *52*, 3673-3676.
6. Kang, H.; Oka, S.; Lee, D. Y.; Park, J.; Aponte, A. M.; Jung, Y. S.; Bitterman, J.; Zhai, P. Y.; He, Y.; Kooshapur, H.; Ghirlando, R.; Tjandra, N.; Lee, S. B.; Kim, M. K.; Sadoshima, J.; Chung, J. H. Sirt1 Carboxyl-Domain is an ATP-Repressible Domain that is Transferrable to Other Proteins. *Nat. Commun.* **2017**, 15560.
7. Chen, L. Z.; Chao, J.; Qu, X. M.; Zhang, H. B.; Zhu, D.; Su, S.; Aldalbahi, A.; Wang, L. H.; Pei, H. Probing Cellular Molecules with PolyA-Based Engineered

Aptamer Nanobeacon. *ACS Appl. Mater. Interfaces* **2017**, *9*, 8014-8020.

8. Meng, H. M.; Zhang, X. B.; Lv, Y. F.; Zhao, Z. L.; Wang, N. N.; Fu, T.; Fan, H. H.; Liang, H.; Qiu, L. P.; Zhu, G. Z.; Tan, W. H. DNA Dendrimer: An Efficient Nanocarrier of Functional Nucleic Acids for Intracellular Molecular Sensing. *ACS Nano* **2014**, *6*, 6171-6181.
9. Lu, S. S.; Hu, T.; Wang, S.; Sun, J.; Yang, X. R. Ultra-Sensitive Colorimetric Assay System Based on the Hybridization Chain Reaction-Triggered Enzyme Cascade Amplification. *ACS Appl. Mater. Interfaces* **2017**, *9*, 167-175.
10. Su, S.; Sun, H. F.; Cao, W. F.; Chao, J.; Peng, H. Z.; Zuo, X. L.; Yuwen, L. H.; Fan, C. H.; Wang, L. H. Dual-Target Electrochemical Biosensing Based on DNA Structural Switching on Gold Nanoparticle-Decorated MoS_2 Nanosheets. *ACS Appl. Mater. Interfaces* **2016**, *8*, 6826-6833.
11. Dong, Y. P.; Zhou, Y.; Wang, J.; Zhu, J. J. Electrogenerated Chemiluminescence Resonance Energy Transfer between $Ru(bpy)_3^{2+}$ Electrogenerated Chemiluminescence and Gold Nanoparticles/Graphene Oxide Nanocomposites with Graphene Oxide as Coreactant and Its Sensing Application. *Anal. Chem.* **2016**, *88*, 5469-5475.
12. Song, Y. H.; Yang, X.; Li, Z. Q.; Zhao, Y. J.; Fan, A. P. Label-Free Chemiluminescent ATP Aptasensor Based on Graphene Oxide and an Instantaneous Derivatization of Guanine Bases. *Biosens. Bioelectron.* **2014**, *51,* 232-237.
13. Chen, D.; Zhang, H.; Li, X.; Li, J. H. Biofunctional Titania Nanotubes for

Visible-Light-Activated Photoelectrochemical Biosensing. *Anal. Chem.* **2010**, *82*, 2253-2261.

14. Wang, L. N.; Han, D. X.; Ni, S.; Ma, W. G.; Wang, W.; Niu, L. Photoelectrochemical Device Xased on Mo-Doped $BiVO_4$ Enables Smart Analysis of the Global Antioxidant Capacity in Food. *Chem. Sci.* **2015**, *6*, 6632-6638.
15. Zhao, W. W.; Xu, J. J.; Chen, H. Y. Photoelectrochemical DNA Biosensors. *Chem. Rev.* **2014**, *114*, 7421-7441.
16. Du, J.; Liu, M. Y.; Lou, X. H.; Zhao, T.; Wang, Z.; Xue, Y.; Zhao, J. L.; Xu, Y. S. Highly Sensitive and Selective Chip-Based Fluorescent Sensor for Mercuric Ion: Development and Comparison of Turn-On and Turn-Off Systems. *Anal. Chem.* **2012**, *84*, 8060-8066.
17. Kumar, P. N.; Narayanan, R.; Deepa, M.; Srivastava, A. K. Au@poly(acrylic acid) Plasmons and C_{60} Improve the Light Harvesting Capability of a TiO_2/CdS/CdSeS Photoanode. *J. Mater. Chem. A* **2014**, *2*, 9771-9783.
18. Hu, C. G.; Zheng, J. N.; Su, X. Y.; Wang, J.; Wu, W. Z.; Hu, S. S. Ultrasensitive All-Carbon Photoelectrochemical Bioprobes for Zeptomole Immunosensing of Tumor Markers by an Inexpensive Visible Laser Light. *Anal. Chem.* **2013**, *85*, 10612-10619.
19. Zhang, K. N.; Zhang, T. N.; Cheng, G. H.; Li, T. X.; Wang, S. X.; Wei, W.; Zhou, X. H.; Yu, W. W.; Sun, Y.; Wang, P.; Zhang, D.; Zeng, C. G.; Wang, X. J.; Hu, W. D.; Fan, H. J.; Shen, G. Z.; Chen, X.; Duan, X. F.; Chang, K.; Dai, N. Interlayer

Transition and Infrared Photodetection in Atomically Thin Type-II $MoTe_2/MoS_2$ van der Waals Heterostructures. *ACS Nano* **2016**, *10*, 3852-3858.

20. Xu, S. J.; Li, D.; Wu, P. Y. One-Pot, Facile, and Versatile Synthesis of Monolayer MoS_2/WS_2 Quantum Dots as Bioimaging Probes and Efficient Electrocatalysts for Hydrogen Evolution Reaction. *Adv. Funct. Mater.* **2015**, *25*, 1127-1136.
21. Yan, J.; Chen, Z. G.; Ji, H. Y.; Liu, Z.; Wang, X.; Xu, Y. G.; She, X. J.; Huang, L. Y.; Xu, L.; Xu, H.; Li, H. M. Construction of a 2D Graphene-Like MoS_2/C_3N_4 Heterojunction with Enhanced Visible-Light Photocatalytic Activity and Photoelectrochemical Activity. *Chem. Eur. J.* **2016**, *22*, 4764-4773.
22. Fan, G. C.; Zhu, H.; Du, D.; Zhang, J. R.; Zhu, J. J.; Lin, Y. H. Enhanced Photoelectrochemical Immunosensing Platform Based on CdSeTe@CdS:Mn Core-Shell Quantum Dots-Sensitized TiO_2 Amplified by CuS Nanocrystals Conjugated Signal Antibodies. *Anal. Chem.* **2016**, *88*, 3392-3399.
23. Wang, G. L.; Shu, J. X.; Dong, Y. M.; Wu, X. M.; Zhao, W. W.; Xu, J. J.; Chen, H. Y. Using G-Quadruplex/Hemin To "Switch-On" the Cathodic Photocurrent of p-Type PbS Quantum Dots: Toward a Versatile Platform for Photoelectrochemical Aptasensing. *Anal. Chem.* **2015**, *87*, 2892-2900.
24. Nair, G.; Chang, L. Y.; Geyer, S. M.; Bawendi, M. G. Perspective on the Prospects of a Carrier Multiplication Nanocrystal Solar Cell. *Nano Lett.* **2011**, *11*, 2145-2151.
25. Wang, H. J.; Bai, L. J.; Chai, Y. Q.; Yuan, R. Synthesis of Multi-Fullerenes Encapsulated Palladium Nanocage, and Its Application in

Electrochemiluminescence Immunosensors for the Detection of Streptococcus Suis Serotype 2. *Small* **2014**, *10*, 1857-1865.

26. Khawula, T. N. Y.; Raju, K.; Franklyn, P. J.; Sigalasa, I.; Ozoemena, K. I. Symmetric Pseudocapacitors Based on Molybdenum Disulfide (MoS_2)-modified Carbon Nanospheres: Correlating Physicochemistry and Synergistic Interaction on Energy Storage. *J. Mater. Chem. A* **2016**, *4*, 6411-6425.
27. Cao, S. W.; Yin, Z.; Barber, J.; Boey, F. Y. C.; Loo, S. C. J.; Xue, C. Preparation of Au-$BiVO_4$ Heterogeneous Nanostructures as Highly Efficient Visible-Light Photocatalysts. *ACS Appl. Mater. Interfaces* **2012**, *4*, 418-423.
28. Xie, S. B.; Dong, Y. W.; Yuan, Y. L.; Chai, Y. Q.; Yuan, R. Ultrasensitive Lipopolysaccharides Detection Based on Doxorubicin Conjugated N-(Aminobutyl)-N-(ethylisoluminol) as Electrochemiluminescence Indicator and Self-Assembled Tetrahedron DNA Dendrimers as Nanocarriers. *Anal. Chem.* **2016**, *88*, 5218-5224.
29. Zhang, Z. X.; Balogh, D.; Wang, F.; Willner, I. Smart Mesoporous SiO_2 Nanoparticles for the DNAzyme-Induced Multiplexed Release of Substrates. *J. Am. Chem. Soc.* **2013**, *135*, 1934-1940.
30. Zhang, H. Q.; Lai, M. D.; Zuehlke, A.; Peng, H. Y.; Li, X. F.; Le, X. C. Binding-Induced DNA Nanomachines Triggered by Proteins and Nucleic Acids. *Angew. Chem. Int. Ed.* **2015**, *54*, 14326-14330.
31. Ren, X. P.; Pang, L. Q.; Zhang, Y. X.; Ren, X. D.; Fanac, H. B.; Liu, S. Z. One-Step Hydrothermal Synthesis of Monolayer MoS_2 Quantum Dots for Highly

Efficient Electrocatalytic Hydrogen Evolution. *J. Mater. Chem. A* **2015**, *3*, 10693-10697.

32. Shi, Y.; Wang, J.; Wang, C.; Zhai, T. T.; Bao, W. J.; Xu, J. J.; Xia, X. H.; Chen, H. Y. Hot Electron of Au Nanorods Activates the Electrocatalysis of Hydrogen Evolution on MoS_2 Nanosheets. *J. Am. Chem. Soc.* **2015**, *137*, 7365-7370.
33. Zhao, W. W.; Tian, C. Y.; Xu, J. J.; Chen, H. Y. The Coupling of Localized Surface Plasmon Resonance-Based Photoelectrochemistry and Nanoparticle Size Effect: towards Novel Plasmonic Photoelectrochemical Biosensing. *Chem. Commun.* **2012**, *48*, 895-897.
34. Zhou, H.; Han, T. Q.; Wei, Q.; Zhang, S. S. Efficient Enhancement of Electrochemiluminescence from Cadmium Sulfide Quantum Dots by Glucose Oxidase Mimicking Gold Nanoparticles for Highly Sensitive Assay of Methyltransferase Activity. *Anal. Chem.* **2016**, *88*, 2976-2983.
35. Pestryakov, A. N.; Lunin, V. V.; Kharlanov, A. N.; Kochubey, D. I.; Bogdanchikova, N.; Stakheev, A. Y. Influence of Modifying Additives on Electronic State of Supported Gold. *Journal of Molecular Structure* **2002**, *642*, 129-136.
36. .Deng, W. L.; Carpenter, C.; Yi, N.; Stephanopoulos, M. F. Comparison of the Activity of Au/CeO_2 and Au/Fe_2O_3 Catalysts for the CO Oxidation and the Water-Gas Shift Reactions. *Topics in Catalysis* **2007**, *44*, 1-2.
37. Zhen, J. M.; Liu, Q.; Chen, X.; Li, D.; Qiao, Q. Q.; Lu, Y. L.; Yang, S. F. An Ethanolamine-Functionalized Fullerene as an Efficient Electron Transport Layer

for High-Efficiency Inverted Polymer Solar Cells. *J. Mater. Chem. A* **2016**, *4*, 8072-8079.

38. Akter, R.; Jeong, B. J.; Choi, J. S.; Rahman, M. A. Ultrasensitive Nanoimmunosensor by Coupling Non-Covalent Functionalized Graphene Oxide Platform and Numerous Ferritin Labels on Carbon Nanotubes. *Biosens. Bioelectron.* **2016**, *80*, 123-130.
39. Bai, L. J.; Yuan, R.; Chai, Y. Q.; Zhuo, Y.; Yuan, Y. L.; Wang, Y. Simultaneous Electrochemical Detection of Multiple Analytes Based on Dual Signal Amplification of Single-Walled Carbon Nanotubes and Multi-Labeled Grapheme Sheets. *Biomaterials* **2012**, *33*, 1090-1096.
40. Yan, H. H.; Song, P.; Zhang, S.; Zhang, J.; Yang, Z. X.; Wang, Q. A Low Temperature Gas Sensor Based on Au-Loaded MoS_2 Hierarchical Nanostructures for Detecting Ammonia. *Ceramics International* **2016**, *42*, 9327-9331.
41. Liu, Y. T.; Wang, H. J.; Xiong, C. Y.; Yuan, Y. L.; Chai, Y. Q.; Yuan, R. A Sensitive Electrochemiluminescence Immunosensor Based on Luminophore Capped Pd@Au Core-Shell Nanoparticles as Signal Tracers and Ferrocenyl Compounds as Signal Enhancers. *Biosens. Bioelectron.* **2016**, *81*, 334-340.
42. Huo, Z. Y.; Tsung, C. K.; Huang, W. Y.; Zhang, X. F.; Yang, P. D. Sub-Two Nanometer Single Crystal Au Nanowires. *Nano Lett.* **2008**, *8*, 2041-2044.
43. Miao, Y. Y.; Xu, J.; Shen, Y.; Chen, L.; Bian, Y. P.; Hu, Y.; Zhou, W.; Zheng, F.; Man, N.; Shen, Y. Y.; Zhang, Y. J.; Wang, M.; Wen, L. P. Nanoparticle as Signaling Protein Mimic: Robust Structural and Functional Modulation of

CaMKII upon Specific Binding to Fullerene C_{60} Nanocrystals. *ACS Nano* **2014**, *8*, 6131-6144.

44. Kim, K.; Lee, T. H.; Santos, E. J. G.; Jo, P. S.; Salleo, A.; Nishi, Y.; Bao, Z. N. Structural and Electrical Investigation of C_{60} Graphene Vertical Heterostructures. *ACS Nano* **2015**, *9*, 5922-5928.
45. An, T.; Tang, J.; Zhang, Y. Y.; Quan, Y. Z.; Gong, X. G.; Al-Enizi, A. M.; Elzatahry, A. A.; Zhang, L. J.; Zheng, G. F. Photoelectrochemical Conversion from Graphitic C_3N_4 Quantum Dot Decorated Semiconductor Nanowires. *ACS Appl. Mater. Interfaces* **2016**, *8*, 12772-12779.
46. Zhao, M.; Fan, G. C.; Chen, J. J.; Shi, J. J.; Zhu, J. J. Highly Sensitive and Selective Photoelectrochemical Biosensor for Hg^{2+} Detection Based on Dual Signal Amplification by Exciton Energy Transfer Coupled with Sensitization Effect. *Anal. Chem.* **2015**, *87*, 12340-12347.

For TOC only

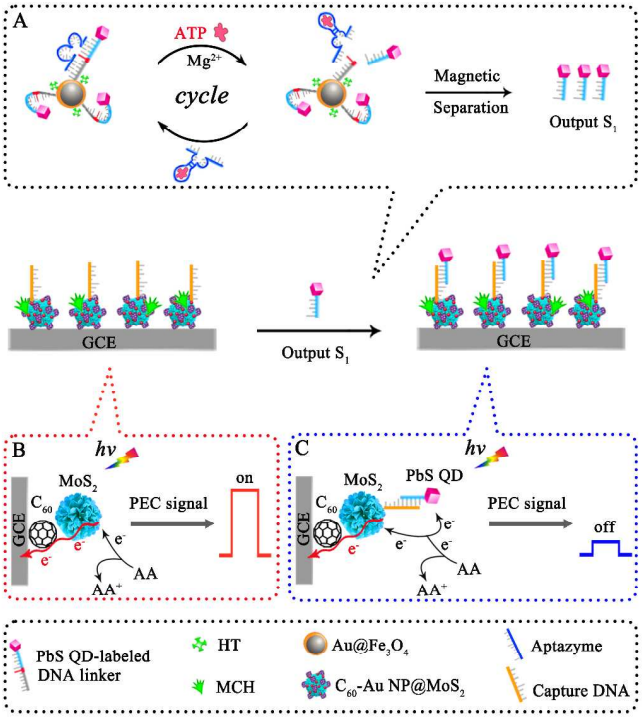
A
ATP
Mg2+
cycle
Magnetic
Separation
Output S1
GCE
Output S1
GCE
B
hv
MoS2
C60
GCE
PEC signal
on
e-
AA
AA+
C
hv
MoS2
PbS QD
C60
GCE
PEC signal
off
e-
AA
AA+
PbS QD-labeled
DNA linker
HT
MCH
Au@Fe3O4
C60-Au NP@MoS2
Aptazyme
Capture DNA